Influence of MoSi2 on oxidation protective ability of TaB2-SiC coating in oxygen-containing environments within a broad temperature range

Xuanru Ren (XuanruRen@163.com)
China University of Mining and Technology
Junshuai Lv
China University of Mining and Technology
Wei Li
China University of Mining and Technology
Yuwen Hu
China University of Mining and Technology
Ke Sun
China University of Mining and Technology
Can Ma
China University of Mining and Technology
Hongao Chu
China University of Mining and Technology
Weiguang Wang
China University of Mining and Technology
Leihua Xu (xuleihua@cumt.edu.cn)
China University of Mining and Technology
Ziyu Li
China University of Mining and Technology
Peizhong Feng (fengroad@163.com)
China University of Mining and Technology

Research Article

Keywords: MoSi2, TaB2-SiC, Coating, Liquid phase sintering, Compound glass layer, Relative oxygen permeability

Posted Date: March 31st, 2020

DOI: https://doi.org/10.21203/rs.3.rs-19696/v1

Version of Record: A version of this preprint was published at Journal of Advanced Ceramics on August 13th, 2020. See the published version at https://doi.org/10.1007/s40145-020-0406-5.

Abstract

TaB2-SiC coating modified by different content of MoSi2 was fabricated on graphite substrate with SiC inner coating by liquid phase sintering to elevate the anti-oxidation capability of the TaB2-SiC coatings. As compared to the sample with the TaB2-40wt.%SiC coating, the coating sample modified with MoSi2 exhibited a weight gain trend at lower temperatures, the fastest weight loss rate went down by 76%, and the relative oxygen permeability value reduced from about 1% to near 0. More importantly, the large amount of SiO2 glass phase produced over the coating during oxidation was in contact with the modification of MoSi2 , which was proved to be beneficial to the dispersion of Ta-oxides. A concomitantly formed continuous Ta-Si-O-B compound glass layer showed excellent capacity to prevent oxygen penetration. However, when the TaB2 content was sacrificed to increase the MoSi2 content, the relative oxygen permeability of the coating increased instead of decreased. Thus, on the basis of ample TaB2 content, increasing the MoSi2 content of the coating is conducive to reducing the relative oxygen permeability of the coatings in a broad temperature region.

1. Introduction

Carbon materials, especially carbon/carbon composites are deemed to be the most potential materials in the field of aerospace and aeronautical owing to their superior high-temperature mechanical properties, for instance, low coefficient of thermal expansion, outstanding thermal shock resistance, high strength at extreme temperature and so on [1-4]. Unfortunately, the defect that carbon materials easily fail above 500 ℃ due to the oxidation of carbon is unable to be ignored [5], which causes the applications of carbon materials are severely hampered in an oxygen-containing environment. At present, in order to cope with this imperative problem, ceramic coating technology is widely applied to avoid the oxidation of carbon materials in a wide temperature range as much as possible.

It has been commonly accepted that ultra-high temperature ceramics ($UHTC_S$) with high hardness, high melting point and outstanding thermal conductivity are extensively utilized as structure materials in rocket nozzles and other components that work in extreme high temperature environments [6-9]. Moreover, $UHTC_S$ have attracted the attention of many scholars in the field of anti-oxidation coatings, because the refractory oxide formed during the oxidation process will effectively enhance the stability of the compound oxide layer [10,11].

As one of $UHTC_S$, TaB_2 possesses a great deal of outstanding properties including extremely high melting point (3200 °C), high hardness (24.5 GPa), and excellent chemical stability [12,13]. Up till now, numerous TaB_2-added coatings have been fabricated to protect carbon substrates from oxidation. For example, Jiang et al. [14] fabricated a single-layer TaB_2-SiC-Si coating on graphite surface by in-situ reaction and impregnation method to defend graphite materials against oxidation. The results of the oxidation test at 1550 ℃ for 168 h showed that the SiO_2 and Ta_2O_5 layers formed on the outer layer caused 2% mass gain. In view of this, oxidation products played a key role in excellent protection of the coating. Qu et al. [15] prepared a dense TaB_2-SiC coating by pack cementation method to protect C/C composites from oxidation, and the ablation behavior of the samples was investigated. The results that the linear ablation rate for 30 s was 4.2 μm/s illustrated the unique oxidation-inhibition capability of the coating, which was associated with the generation of a Ta-Si-O compound glass layer. Therefore, TaB_2 is an ideal candidate for protecting carbon materials in high-temperature aerobic atmosphere. This is not only because the B_2O_3 layer formed provided fine protection below

1100 ℃, but also because the Ta-Si-O compound glass layer with strong stability in higher temperatures was generated when TaB_2 was introduced into the Si-based coatings [16-18]. But frankly speaking, the oxidation protective capacity of the fabricated TaB_2-SiC coating still needs to be improved.

It's common knowledge that Si-based coatings are broadly exploited to the oxidation protection for carbon materials because of the generation of abundant SiO_2 glass phase on the coating surface at high temperatures. The SiO_2 glass phase created an impactful barrier to oxygen and filled the gap between refractory oxide skeletons [19-21]. Thus, adding sorts of silicide into ultra-high temperature ceramics to construct compound coatings is considered as an effective route. SiC has a similar thermal expansion coefficient as carbon materials, so it is commonly used in the construction of anti-oxidation coatings [22]. However, since a large amount of gas products, such as CO_2 and CO, are released during the oxidation of SiC, large bubbles formed will expose a fresh surface after bursting, and channels for oxygen diffusion will also be formed, which will reduce the protective effect of the glass film [23]. As one of multitudinous silicides, $MoSi_2$ is a kind of material with dual characteristics of metal and ceramic, and it is able to produce a continuous SiO_2 glass layer to protect its substrate from oxidation at temperatures as high as 1700 ℃ [24]. As a result, it has already been used in the preparation of electric heating elements. Conceivably, $MoSi_2$ is regarded as a high temperature anti-oxidation coating material [25]. At present, a number of coatings based on $MoSi_2$ have been prepared to protect carbon materials from oxidation. Huang et al. [26] prepared an outer $MoSi_2$ layer on SiC inner layer by hydrothermal electrophoretic deposition to protect C/C composites. After undergoing isothermal oxidation tests at 1500 ℃ for 346 h, the sample possessed a weight loss of 2.49 $mg \cdot cm^{-2}$. Wu et al. [27] fabricated a $MoSi_2$-based coating composed of $MoSi_2$, Mo_5Si_3 and SiO_2 on the surface of SiC inner coating by supersonic plasma spraying to defend C/C composites against oxidation. After oxidation tests for more than 400 h at 1500 ℃, the result showed that the weight loss of the specimen was only 1.14%. Briefly, the excellent oxidation protective performance shown by these coatings is ascribed to the generation of a continuous SiO_2 glass layer on the coating surface. In addition, $MoSi_2$ as a sintering aid can effectively increase the density of the coatings [28,29], which can decelerate further corrosion of the coating by oxygen.

At the moment, because of the fact that $MoSi_2$ possesses superior anti-oxidation performance, $MoSi_2$-added UHTC coatings, such as the ZrB_2-$MoSi_2$-SiC coating [30-32] and the HfB_2-$MoSi_2$-SiC coating [33], have attracted lots of attention. Yet, until now, few studies have been able to elaborate the unique role of $MoSi_2$ in multiphase coating. Consequently, in this paper, $MoSi_2$ was used as the second silicon source, and a TaB_2-$MoSi_2$-SiC coating was fabricated. In detail, the influence of $MoSi_2$ modification on the oxidation protective capacity of the coatings in an oxygen-containing atmosphere within a wide temperature region and the generation mechanisms of the compound glass layer were studied.

In addition, in order to synthesis the coatings that can provide long-term protection for carbon materials, the liquid phase sintering method has been widely applied in our previous work [34], which is an ideal method because the content of various components in the coatings can be adjusted so that a coating with better oxidation resistance is available. Likewise, in this paper, the coatings were synthesized by the combination of liquid phase sintering and in-situ reaction, and the in-situ reaction was introduced to increase the adhesion of the coating to the substrate.

2. Materials And Method

The TaB_2-$MoSi_2$-SiC coatings were fabricated by liquid phase sintering on the SiC buffer layer that was prepared by pack cementation to protect graphite substrates (3mm×3mm×3mm). The raw materials consisted of TaB_2 powders, $MoSi_2$ powders and SiC powders (Licheng Innovation Metal Materials Technology Co., Ltd, Beijing, China), graphite powders (Hongtu Burden Co., Ltd, Liaoyang, China), silicon powders (Yuancheng New Material Industry Group Co., Ltd, Yinchuan, China) and silica sol ($SiO_2 \cdot nH_2O$) (the $M_{other\ raw\ materials} : V_{silica\ sol}$ = 0.6-1.7 g/ml) (City Fire Crystal Glass Co., Ltd, Dezhou, China). It also should be noted that the composite coating consists of an outer layer and an inner SiC buffer layer. Therefore, as schematically represented in Fig. 1, the preparation process of the coatings consists of three steps. First, in order to alleviate the mismatch of the thermal expansion coefficients of the substrate and the outer layer, the inner SiC layer was fabricated by pack cementation which is in widespread use [35]. Second, the raw materials were weighed in different proportions, and then they were mixed as slurries for the preparation of the coatings. Next, brush the prefabricated slurry onto the surface of SiC covered graphite substrate, and dry the specimens at 100 ℃ for half an hour later, repeating the above operation three times. Ultimately, the coatings were sintered at 2100 ℃ for 2 h in argon atmosphere. In addition, partial SiC was formed by in-situ reaction between Si and C.

The phase composition of the coatings before and after oxidation were studied by X-ray diffractometer (Bruker D8 ADVANCE XRD, BRUKER AXS, Germany). Field Emission Scanning Electron Microscopy (JSM-6700F FE-SEM, JEOL, Japan) was used to observe the micro-morphology of the prepared coatings before and after oxidation, and the energy dispersive spectroscopy was applied to analyze the elemental composition of the compound glass layer. To research the dynamic oxidation behavior of the coatings in oxygenated atmosphere from 25 ℃ to 1500 ℃, Thermogravimetric Analyzer (STA 449 F3, TGA, Netzsch, Germany) with a heating rate of 5 ℃/min was employed.

3. Results And Discussion

The XRD pattern of the TaB_2-$MoSi_2$-SiC coating synthesized by liquid phase sintering is displayed in Fig. 2. As shown in Fig. 2, the composite coating contains $MoSi_2$, SiC and TaB_2 phases, illustrating successful preparation of the multiphase coating. In addition, note that there is no other impurity phase in the coating because Si powders and carbon powders both participated in the generation of SiC through in-situ reaction between Si and C.

The BSE image for observing the surface microstructure of the fabricated coating is presented in Fig. 3. According to the results of EDS analysis, the white and grey particles are TaB_2, $MoSi_2$ phases, respectively. What's more, it is evident that these fine particles were distributed evenly over the black SiC layer and embedded in loose SiC inner layer, which is favorable to elevate the oxidation resistance of the fabricated coating. This is because it is desirable that the refractory oxidation products will be uniformly distributed in the SiO_2 glass after the oxidation process.

The cross-sectional backscatter image of the fabricated coating is demonstrated in Fig. 4. Obviously, the fabricated coating consists of two layers and bonds tightly with the graphite substrate, which is attribute to the exceptional preparation method. The first layer is a multiphase coating including TaB_2, $MoSi_2$ and SiC phases

prepared by liquid phase sintering. The second layer is inner SiC fabricated by pack cementation. In addition, there is no distinct gap or void in the interface, which is a prerequisite for the coating providing protection against oxidation to the graphite matrix. Consequently, liquid phase sintering is considered to be an extraordinary method to fabricate the coating with outstanding oxidation protective performance.

The TGA tests of pure graphite substrate and the samples coated by two different coatings were performed in air within a wide temperature range to demonstrate the superior behavior of $MoSi_2$ compared with SiC in the application of anti-oxidation coatings. As shown in Fig. 5 (a), the pure graphite suffered fearful destruction from 700 ℃, but the weight loss of the other samples both presented a marked decrease under the protection of fabricated coatings. With the aim of visually observing the initial oxidation characteristic of the samples, Fig. 5(b) displays the TGA curves from 500 ℃ to 900 ℃. Clearly, the pure graphite began to be oxidized when the temperature reached about 570 ℃, whereas the initial weight loss temperatures of the specimen with the SiC/SiC coating and the specimen with the SiC-$MoSi_2$/SiC coating were around 700 ℃, 900 ℃, respectively. Significantly, the weight loss of the sample with the SiC-$MoSi_2$/SiC coating was lower than that of the sample with the SiC/SiC coating in a wide temperature range, indicating that $MoSi_2$ performed better than SiC when it was applied to the anti-oxidation coating. In addition, the weight change rate curve over a wide temperature range are analyzed to elucidate the anti-oxidation process in detail. As displayed in Fig. 5(c), the fastest weight loss range was from 1000 ℃ to 1300 ℃. The modification of $MoSi_2$ reduced the fastest weight loss rate although it failed to narrow the fastest weight loss region, which decreased the damage of carbon material during oxidation.

Since the oxidation of carbon is the main cause of sample weight loss, the weight loss of the sample to some extent reflects the degree of oxygen penetration into the carbon matrix. Thus, a concept called relative oxygen permeability was proposed to describe the ability of the coating to prevent oxygen penetration in our previous work [36]. Relative oxygen permeability was defined via Eq. (1).

$$RP_{O_2} = \frac{\Delta m_1 \cdot S_2}{\Delta m_2 \cdot S_1} \times 100\% \qquad (1)$$

Δm_1: Weight change of the sample covered by fabricated coating

Δm_2: Weight change of the pure carbon sample

S_1: Superficial area of the sample covered by fabricated coating

S_2: Superficial area of the pure carbon sample

The weight loss of the substrate was primarily concentrated in the fastest weight loss region. For purpose of clarifying the capability of $MoSi_2$ to prevent the oxygen delivery from outside to substrate, Fig. 6 shows the relative oxygen permeability of the SiC/SiC coating and the SiC-$MoSi_2$/SiC coating. Owing to the modification of $MoSi_2$, the relative oxygen permeability value of the SiC/SiC coating reduced from about 5% to 3% in the fastest weight loss region, which further demonstrates that $MoSi_2$ plays a noteworthy role in enhancing the oxidation protective ability of the coatings.

Previously, the protective capability of the TaB_2-SiC coating has been investigated [36]. To verify the improvement in the oxidation resistance of the coating modified with $MoSi_2$, TGA tests were performed in an air atmosphere from indoor temperature to 1500 ℃. The samples with different coatings both presented mild weight loss in the initial stage from room temperature to about 650 ℃, as shown in Fig. 7(a). Additionally, the two dynamic oxidation curves didn't display an increasing trend until the temperature reached about 700 ℃. It should be noted, however, that the sample with the TaB_2-20wt.%$MoSi_2$-20wt.%SiC/SiC coating manifested an earlier trend of weight gain due to the addition of $MoSi_2$. And in general, sample weight gain means the formation of passive oxidation products with protective capabilities. Therefore, the formation of an oxide layer at lower temperatures contributes to extend the protective temperature range of the coating. Moreover, the curve representing the sample with the TaB_2-40wt.%SiC/SiC coating showed two different declining tendencies, comprising a relatively rapid decline from 850 ℃ to 1200 ℃ and a gentle decrease from 1200 ℃ to 1500 ℃. In the other hand, evidently, the weight of the sample with the $MoSi_2$ modified coating only decreased slightly after a rapid increase, suggesting that the coating modified with $MoSi_2$ presented better oxidation resistance.

As presented in Fig. 7(b), the fastest weight loss zone of the sample with the TaB_2-40wt.%SiC/SiC coating is wider than that of the $MoSi_2$ modified sample. At the same time, the fastest weight loss rate of the $MoSi_2$ modified sample was descending, compared with that of the sample with the TaB_2-40wt.%SiC/SiC coating. In light of this, coatings with wider protection temperature range and stronger protection capability can be available through $MoSi_2$ modification.

The relative oxygen permeability curve reflects the ability of the coatings to prevent oxygen diffusion. As shown in Fig. 8, it should be emphasized the negative portion of the curve means that the specimen increased in weight relative to the initial state. In the fastest weight loss region, the relative oxygen permeability of the $MoSi_2$ modified coating was lower than that of the TaB_2-40wt.%SiC/SiC coating. Besides, the value of the $MoSi_2$ modified coating approached zero earlier, which means that the coating modified with $MoSi_2$ established a defense against oxygen at a lower temperature. Accordingly, $MoSi_2$ presents superior performance in fending off the oxygen penetration when it is applied to the anti-oxidation coatings.

The XRD pattern of the TaB_2-$MoSi_2$-SiC coating after oxidation is displayed in Fig. 9. The diffraction peaks of several refractory Ta-oxides comprising TaO, TaO_2 and Ta_2O_5 were detected. These Ta-oxides remained stable even at elevated environments. Moreover, the formation of SiO_2 filling cracks and voids was due not only to the oxidation of SiC but also to the oxidation of $MoSi_2$. The SiC peaks remained visible, indicating that the oxide layer was thin, which further illustrated the good protective ability of the coating. Mo_5SiB_2 that is a promising high temperature structure material with superb oxidation and creep resistance was detected after oxidation [37], hence it aids in enhancing the stability of the oxide layer in ultra-high temperature environments. In addition, the existence of B_2SiO_5 is attributed to the reaction between SiO_2 and B_2O_3, and MoO_3 phase were not detected because of evaporation at low temperatures.

In the interest of clarifying the mechanism of improving the oxidation resistance of the coating by $MoSi_2$ modification, the surface microstructure of the TaB_2-40wt.%SiC/SiC coating and the TaB_2-20wt.%$MoSi_2$-20wt.%SiC/SiC coating after TGA tests are displayed in Fig. 10. As presented in Fig. 10(a), it is evident that the Ta-oxides, the grey particles, were uniformly distributed on the coating surface at a low magnification. However,

Fig. 10(b), the magnification of Fig. 10(a), shows the existence of the Ta-oxides aggregate structure which is incapable of greatly improving the stability of the glass layer [38]. In contrast, a novel phenomenon that more SiO_2 glass phase was generated on the coating with $MoSi_2$ modified can be observed from Fig. 10(c). Moreover, it should be noted that the traces of liquid flow and Ta-oxides dispersion can be found distinctly from Fig. 10(d). Numerous tiny Ta-oxides were able to be dispersed in the glass layer on account of the excellent fluidity provided by a large quantity of SiO_2 glass phase. In this case, the outermost glass layer became viscous and stable, providing a more efficient barrier against oxygen than the pure SiO_2 glass layer. Thus, the addition of $MoSi_2$ significantly elevated the oxidation protective property of the coatings. What's more, what the SEM micrographs shows are coincident with the results of the TGA tests.

To study the influence of the $MoSi_2$ content of the coatings on the anti-oxidation performance in a dynamic aerobic environment, the TGA tests of the coatings with different component ratios were carried out. As can be seen in Fig. 11(a), for curve 2,3,4, the weight loss manifested a distinct decrease as a whole in a broad temperature range with the increasing of $MoSi_2$ content in the coatings, indicating that the partial substitution of $MoSi_2$ for SiC significantly improved the oxidation protective performance of the coatings in aerobic environments. On the contrary, the weight loss of the sample with the TaB_2-60wt.%$MoSi_2$-20wt.%SiC/SiC coating is higher than that of the sample with the TaB_2-40wt.%$MoSi_2$-20wt.%SiC/SiC coating, indicating that increasing the amount of $MoSi_2$ excessively at the expense of the TaB_2 content in the construction of anti-oxidation coating cannot lead to a better result. The critical role of TaB_2 in Si-based coatings was illustrated from the other hand.

The weight change rate curves of the coatings are displayed in Fig. 11(b). As shown in curves 2, 3, 4, the effect of $MoSi_2$ modification on narrowing the fastest weight loss region was negligible, but the reduction of the fastest weight loss rate was obvious. Also, the more $MoSi_2$ was added, the more obvious the reducing effect was. In consequence, the damage of the carbon matrix in the fastest weight loss zone was decreasing due to the addition of $MoSi_2$, illustrating that $MoSi_2$ improved the oxidation resistance of the coatings especially in the fastest weight loss zone. In line with Fig. 11(a), the coating with the highest $MoSi_2$ content failed to exhibit the best protection performance. This could be caused by the lack of refractory oxide during the oxidation process. The stability of the glass layer was decreased, although the amount of SiO_2 formed was increased.

In order to describe the effect of $MoSi_2$ content on the capacity of the coating to block oxygen infiltration, Fig. 12 shows the relative oxygen permeability curves of the TaB_2-$MoSi_2$-SiC/SiC coatings with dissimilar $MoSi_2$ or TaB_2 contents. As can be seen in Fig. 12, for curve 2, 3, 4, the relative oxygen permeability of the samples gradually declined with the increasing of $MoSi_2$ content, indicating that the adding of $MoSi_2$ improved the ability of the coating to prevent oxygen infiltration in the fastest weight loss region. In addition, due to the generation of the oxide layer, all the curves tended to gentle in the end, which is consistent with that shown in Fig. 11(a). Nevertheless, as seen in Fig. 12, the relative oxygen permeability of the coatings with high $MoSi_2$ content tended to 0.5% at about 1050 ℃, while other coatings with low $MoSi_2$ content did not reach the same level until 1400 ℃, suggesting that the modification of $MoSi_2$ effectively boosted the formation of the ability to prevent oxygen penetration during the initial stage of oxidation.

After isothermal oxidation tests at 1500 ℃ in an aerobic environment, the SEM micrographs of the coating surface are displayed in Fig. 13. Clearly, there are a large quantity of bulk Ta-oxides on the coating without the addition of $MoSi_2$, which is shown in Fig. 13(a). On the other hand, surprisingly, due to the modification of $MoSi_2$, the aggregation phenomenon of Ta-oxides is negligible as shown in the other figures. Since $MoSi_2$ provided abundant SiO_2 glass phase with wonder quality and high fluidity after its oxidation at high temperature, the bulk aggregated Ta-oxides were separated into nanocrystals under the action of liquid flow. Hereafter, the tiny particles were evenly dispersed in the SiO_2 glass phase. In the end, a compound glass layer, the gray area shown in Fig. 13, was formed. It is the dominant coating protection mechanism that the compound glass layer is responsible for preventing oxygen penetration. As shown in Fig. 13(a), obviously, the compound glass layer failed to completely cover the black glass layer, because the lack of liquid flow during oxidation resulted in the local aggregation of the Ta-oxides. In this case, although the bulk Ta-oxides which were defined as a pinning phase enabled to oblige the cracks to deflect or terminate, numerous cracks were distributed in the black glass region. Clearly, as the $MoSi_2$ content in the coating increased, the area covered by the compound glass layer enlarged. This proves that the modification of $MoSi_2$ significantly improved the oxidation resistance of the coatings. In addition, as can be seen in Fig. 13(c), there are a number of micron scale Ta-oxide particles distributed at the growth interface. These particles provided nuclei for dendrite growth so that the part area of the coating surface was covered by the dendrites. It is beyond disputed that the dendrite structure contributes to the deflection of the cracks and the relaxation of the stress [39]. Furthermore, as show in Fig. 13(d), the compound glass layer covered most of the coating surface because of the addition of 60wt.% $MoSi_2$. But at the same time, lots of gas products such as MoO_3 were released, resulting in the formation of holes as the paths for oxygen transport. Also, the drop in TaB_2 content caused the increasing instability of the compound glass layer. Therefore, excessively increasing the amount of $MoSi_2$ while decreasing the amount of TaB_2 reduced the protective effect of the coating. Thus, on the premise that the amount of TaB_2 is sufficient, the TaB_2-$MoSi_2$-SiC/SiC coating possesses more outstanding oxidation protective property than the TaB_2-SiC/SiC coating.

Based on the discussion above, the compound glass layer consists of the SiO_2 glass phase and particulate refractory oxides dispersed therein. To further illustrate this conclusion, the specific elemental composition of the oxidized coating surface was disclosed by the surface EDS analysis spectrum, which is presented in Fig. 14. As can be seen, the area of the orange circle, the black region, is rich in Si and O elements, illustrating that this area is SiO_2 glass layer that was not covered by the compound glass layer. Even more important, most areas were covered by the continuous compound glass layer that is constituted by Ta, Si, O and B elements. Besides, the presence of B element was not unexpected because B_3SiO_5 phase was detected in the XRD pattern displayed in Fig. 9. Thus, the results of EDS analysis further demonstrated the generation of the Ta-Si-B-O compound glass layer.

4. Conclusions

In conclusion, the liquid phase sintering was used for fabricating the TaB_2-$MoSi_2$-SiC outer coating with no crack or void to enhance protective ability of the TaB_2-SiC coating. The sample with the coating modified by $MoSi_2$ exhibited a weight gain trend at lower temperatures and the fastest weight loss rate of this sample in the

fastest weight loss zone goes down by 76%. After the modification of $MoSi_2$, it was found that more SiO_2 glass phase was generated during the oxidation process. For this reason, bulk Ta-oxides were stripped into tiny nanocrystals more easily, and then the Ta-oxides nanocrystals were diffusely distributed in the SiO_2 glass layer. The Ta-Si-B-O compound glass layer was formed in this way, and it is the key to blocking oxygen infiltration. The addition of $MoSi_2$ availably improved the anti-oxidation performance of the TaB_2-SiC coating when the content of TaB_2 is fixed. Nevertheless, the coating with the highest $MoSi_2$ content but low TaB_2 content failed to present the best anti-oxidation performance because the instability of the compound glass layer increased.

Declarations

Acknowledgements

This work has been supported by the Fundamental Research Funds for the Central Universities (No. 2018GF14).

References

[1] Kumar P, Srivastava VK. Tribological behaviour of C/C-SiC composites-A review. *J Adv Ceram* 2016, **5:** 1-12.

[2] Jacobson NS, Curry DM. Oxidation microstructure studies of reinforced carbon/carbon. *Carbon* 2006, **44:** 1142-1150.

[3] Chu YH, Fu QG, Li HJ, *et al*. SiC coating toughened by SiC nanowires to protect C/C composites against oxidation. *Ceram Int* 2012, **38:** 189-194.

[4] Ren JC, Zhang YL, Zhang J, *et al*. Improving the flexural property and long-lasting anti-ablation performance of the CVD-HfC coating by in-situ growing HfC nanowires. *Ceram Int* 2019, **45:** 24294-24302.

[5] Fu QG, Zhang JP, Zhang ZZ, *et al*. SiC-$MoSi_2$/ZrO_2-$MoSi_2$ coating to protect C/C composites against oxidation. *T Nonferr Metal Soc* 2013, **23:** 2113-2117.

[6] Xue CQ, Zhou HJ, Hu JB, *et al*. Fabrication and microstructure of ZrB_2-ZrC-SiC coatings on C/C composites by reactive melt infiltration using $ZrSi_2$ alloy. *J Adv Ceram* 2018, **7:** 64-71.

[7] Liu D, Liu HH, Ning SS, *et al*. Synthesis of high-purity high-entropy metal diboride powders by boro/carbothermal reduction. *J Am Ceram Soc* 2019, **102:** 7071-7076.

[8] Liu D, Wen TQ, Ye BL, *et al*. Synthesis of superfine high-entropy metal diboride powders. *Scripta Mater* 2019, **167:** 110-114.

[9] Liu D, Wen T, Ye B, *et al*. Molten salt synthesis, characterization, and formation mechanism of superfine $(Hf_xZr_{1-x})B_2$ solid-solution powders. *J Am Ceram Soc* 2019, **102:** 3763-3770.

[10] Jiang Y, Liu T, Ru H, *et al*. Oxidation and ablation protection of double layer HfB_2-SiC-Si/SiC-Si coating for graphite materials. *J Alloys Compd* 2019, **782:** 761-771.

[11] Wang L, Fu QG, Liu NK, *et al*. Supersonic plasma sprayed $MoSi_2$–ZrB_2 antioxidation coating for SiC–C/C composites. *Surf Eng* 2016, **32:** 508-513.

[12] Licheri R, Orrù R, Musa C, *et al*. Efficient Technologies for the Fabrication of Dense TaB_2-Based Ultra-High-Temperature Ceramics. *ACS Appl Mater Inter* 2010, **2:** 2206-2212.

[13] Zhang X, Hilmas GE, Fahrenholtz WG. Synthesis, densification, and mechanical properties of TaB_2. *Mater Lett* 2008, **62:** 4251-4253.

[14] Jiang Y, Liu T, Ru H, *et al*. Ultra-high-temperature ceramic TaB_2-SiC-Si coating by impregnation and in-situ reaction method to prevent graphite materials from oxidation and ablation. *Ceram Int* 2019, **45:** 6541-6551.

[15] Qu JL, Fu QG, Zhang JP, *et al*. Ablation behavior of TaB_2-SiC coating for carbon/carbon composites under oxyacetylene torch. *Vacuum* 2016, **131:** 223-230.

[16] Li L, Li H, Yin X, *et al*. Oxidation protection and behavior of in-situ zirconium diboride-silicon carbide coating for carbon/carbon composites. *J Alloys Compd* 2015, **645:** 164-170.

[17] Feng T, Li HJ, Shi XH, *et al*. Sealing role of B_2O_3 in $MoSi_2$-$CrSi_2$-Si/B-modified SiC coating for C/C composites. *Corros Sci* 2012, **60:** 4-9.

[18] Fu QG, Li HJ, Wang YJ, *et al*. B_2O_3 modified SiC–$MoSi_2$ oxidation resistant coating for carbon/carbon composites by a two-step pack cementation. *Corros Sci* 2009, **51:** 2450-2454.

[19] Chen P, Zhu L, Ren XR, *et al*. Preparation of oxidation protective $MoSi_2$–SiC coating on graphite using recycled waste $MoSi_2$ by one-step spark plasma sintering method. *Ceram Int* 2019, **45:** 22040-22046.

[20] Li SP, Zhang MY, Huang D, *et al*. Preparation and antioxidation property of a SiC-$MoSi_2$-Si multilayer coating on a C/C composite. *New Carbon Mater* 2018, **33:** 82-87.

[21] Li CY, Li GB, Ouyang H, *et al*. ZrB_2 particles reinforced glass coating for oxidation protection of carbon/carbon composites. *J Adv Ceram* 2019, **8:** 102-111.

[22] Huang JF, Zeng XR, Li HJ, *et al*. Influence of the preparation temperature on the phase, microstructure and anti-oxidation property of a SiC coating for C/C composites. *Carbon* 2004, **42:** 1517-1521.

[23] Fu QG, Li HJ, Shi XH, *et al*. Silicon carbide coating to protect carbon/carbon composites against oxidation. *Carbon* 2005, **52:** 923-927.

[24] Ma QS, Cai LH. Fabrication and oxidation resistance of mullite/yttrium silicate multilayer coatings on C/SiC composites. *J Adv Ceram* 2017, **6:** 360-367.

[25] Zhu L, Zhu YS, Ren XR, *et al*. Microstructure, properties and oxidation behavior of $MoSi_2$-MoB-ZrO_2 coating for Mo substrate using spark plasma sintering. *Surf Coat Technol* 2019, **375:** 773-781.

[26] Huang JF, Wang B, Li HJ, *et al*. A $MoSi_2$/SiC oxidation protective coating for carbon/carbon composites. *Corros Sci* 2011, **53:** 834-839.

[27] Wu H, Li HJ, Ma C, *et al*. $MoSi_2$-based oxidation protective coatings for SiC-coated carbon/carbon composites prepared by supersonic plasma spraying. *J Eur Ceram Soc* 2010, **30:** 3267-3270.

[28] Sciti D, Silvestroni L, Nygren M. Spark plasma sintering of Zr- and Hf-borides with decreasing amounts of $MoSi_2$ as sintering aid. *J Eur Ceram Soc* 2008, **28:** 1287-1296.

[29] Ghaffari SA, Faghihi-Sani MA, Golestani-Fard F, *et al*. Spark plasma sintering of TaC-HfC UHTC via disilicides sintering aids. *J Eur Ceram Soc* 2013, **33:** 1479-1484.

[30] Fu QG, Jing JY, Tan BY, *et al*. Nanowire-toughened transition layer to improve the oxidation resistance of SiC-$MoSi_2$-ZrB_2 coating for C/C composites. *Corros Sci* 2016, **111:** 259-266.

[31] Wang L, Fu QG , Zhao FL, *et al*. A novel gradient SiC-ZrB_2-$MoSi_2$ coating for SiC coated C/C composites by supersonic plasma spraying. *Surf Coat Technol* 2017, **313:** 63-72.

[32]Yao XY, Li HJ, Zhang YL, *et al*. Oxidation and Mechanical Properties of SiC/SiC-$MoSi_2$-ZrB_2 Coating for Carbon/Carbon Composites. *J Mater Sci Technol* 2014, **30:** 123-127.

[33] Wang PP, Li HJ, Ren XR, *et al*. HfB_2-SiC-$MoSi_2$ oxidation resistance coating fabricated through in-situ synthesis for SiC coated C/C composites. *J Alloys Compd* 2017, **722:** 69-76.

[34] Ren XR, Wang LF, Feng PZ, *et al*. Preparation of TaB_2-SiC oxidation protective coating for carbon materials by liquid phase sintering. *Ceram Int* 2018, **44:** 10708-10715.

[35] Ren XR, Li HJ, Chu YH, *et al*. Preparation of oxidation protective ZrB_2-SiC coating by in-situ reaction method on SiC-coated carbon/carbon composites. *Surf Coat Technol* 2014, **247:** 61-67.

[36] Ren XR, Wang WH, Chen P, *et al*. Investigations of TaB_2 on oxidation-inhibition property and mechanism of Si-based coatings in aerobic environment with broad temperature region for carbon materials. *J Eur Ceram Soc* 2019, **39:** 4554-4564.

[37] Lemberg JA, Ritchie RO. Mo-Si-B Alloys for Ultrahigh-Temperature Structural Applications. *Adv Mater* 2012, **24:** 3445-3480.

[38] Ren XR, Wang LF, Feng PZ, *et al*. Low temperature synthesis of pure phase TaB_2 powders and its oxidation protection modification behaviors for Si-based ceramic coating in dynamic oxidation environments. *Ceram Int* 2018, **44:** 15517-15525.

[39] Ren XR, Wang WH, Shang TQ, *et al*. Dynamic oxidation protective ultrahigh temperature ceramic TaB_2-20%wtSiC composite coating for carbon material. *Composites Part B* 2019, **161:** 220-227.

Figures

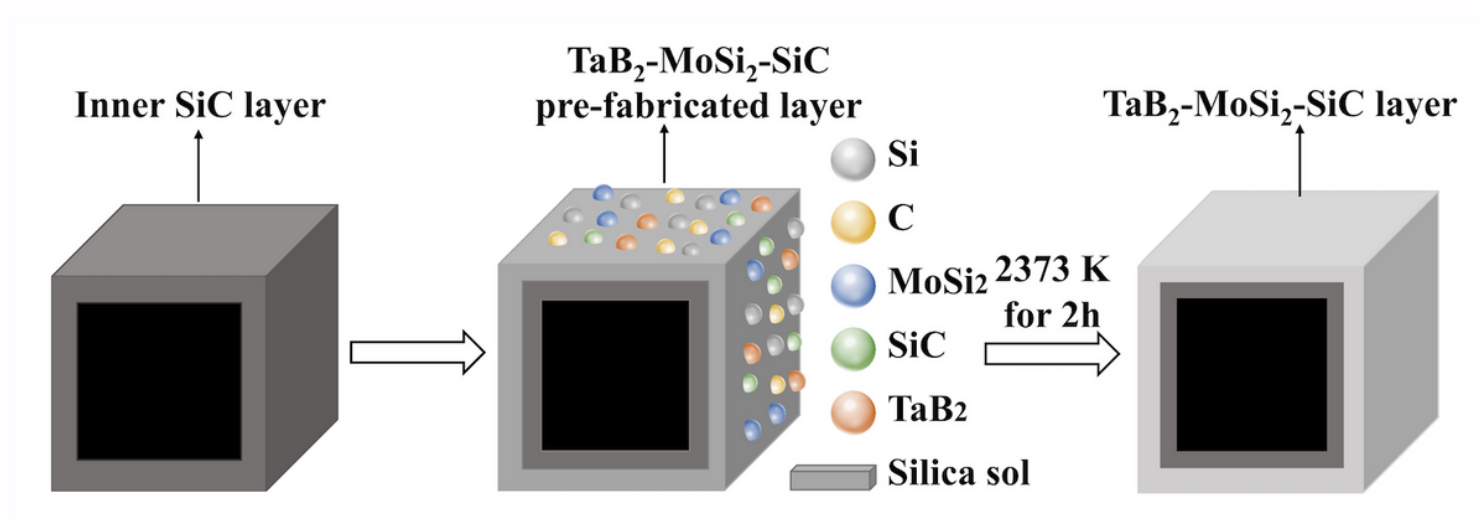

Figure 1

The fabricating process of the TaB2-SiC-MoSi2 coatings.

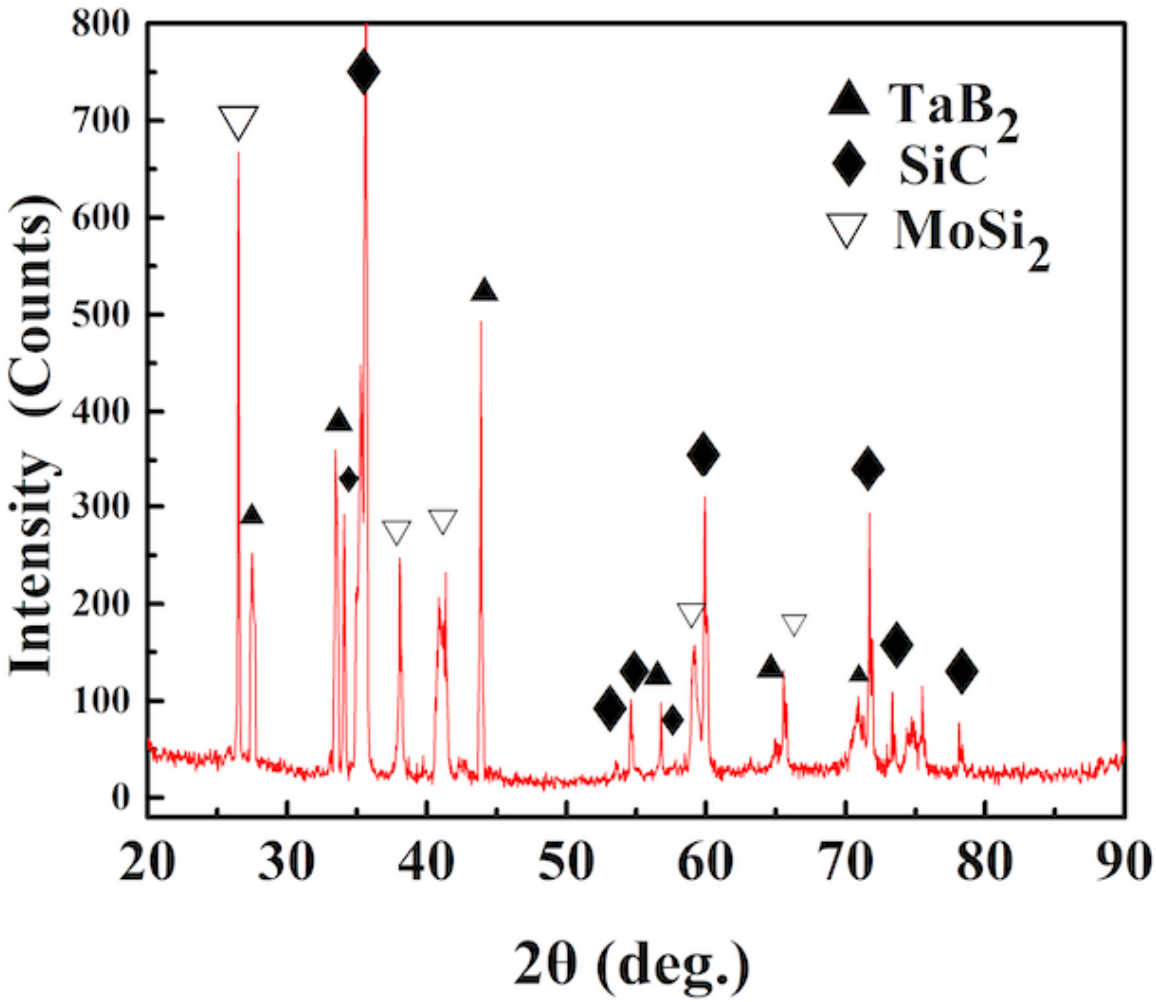

Figure 2

XRD pattern of the TaB2-MoSi2-SiC coating fabricated by liquid phase sintering.

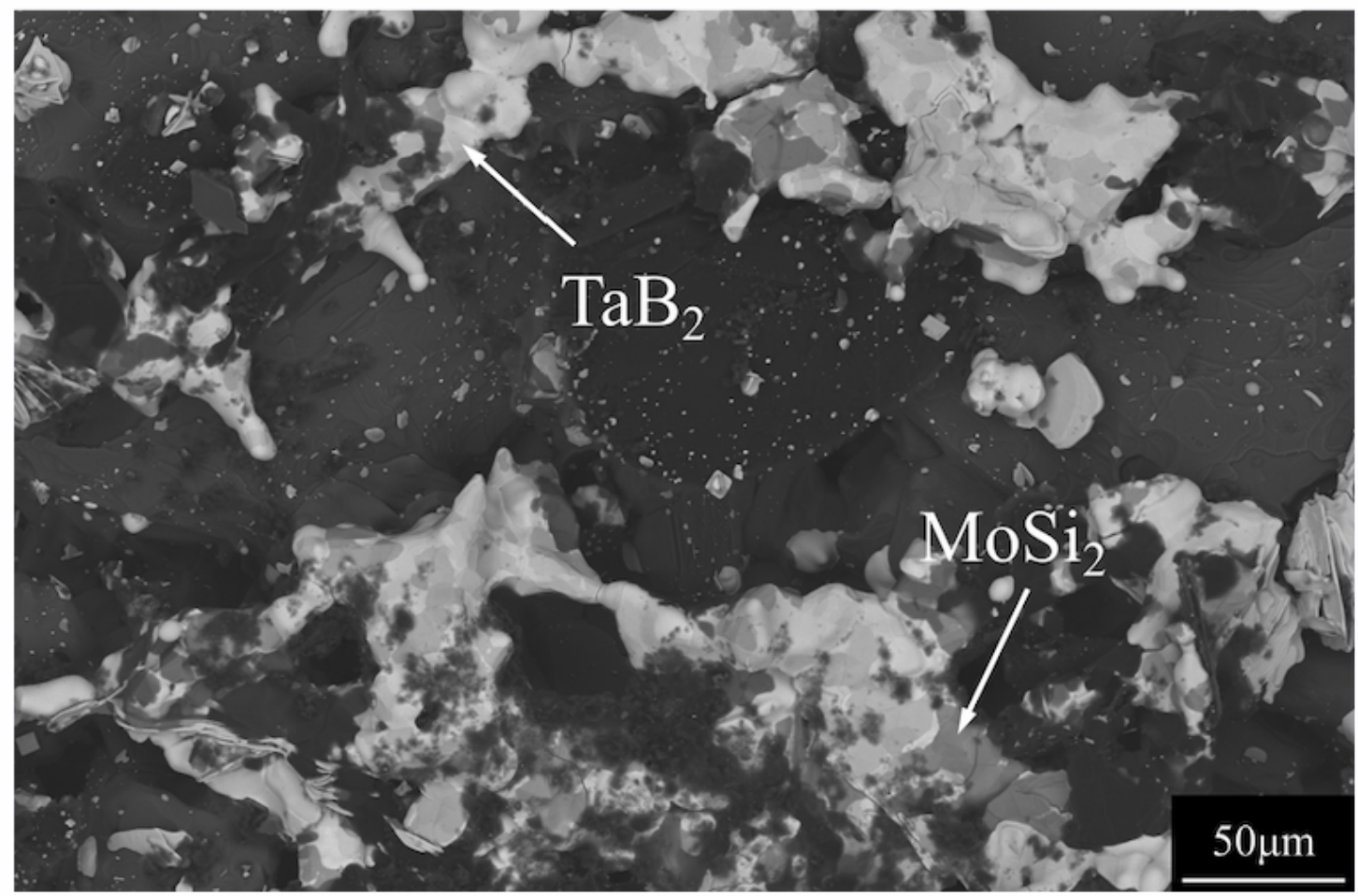

Figure 3

Surface backscatter SEM micrograph of the TaB2-MoSi2-SiC coating.

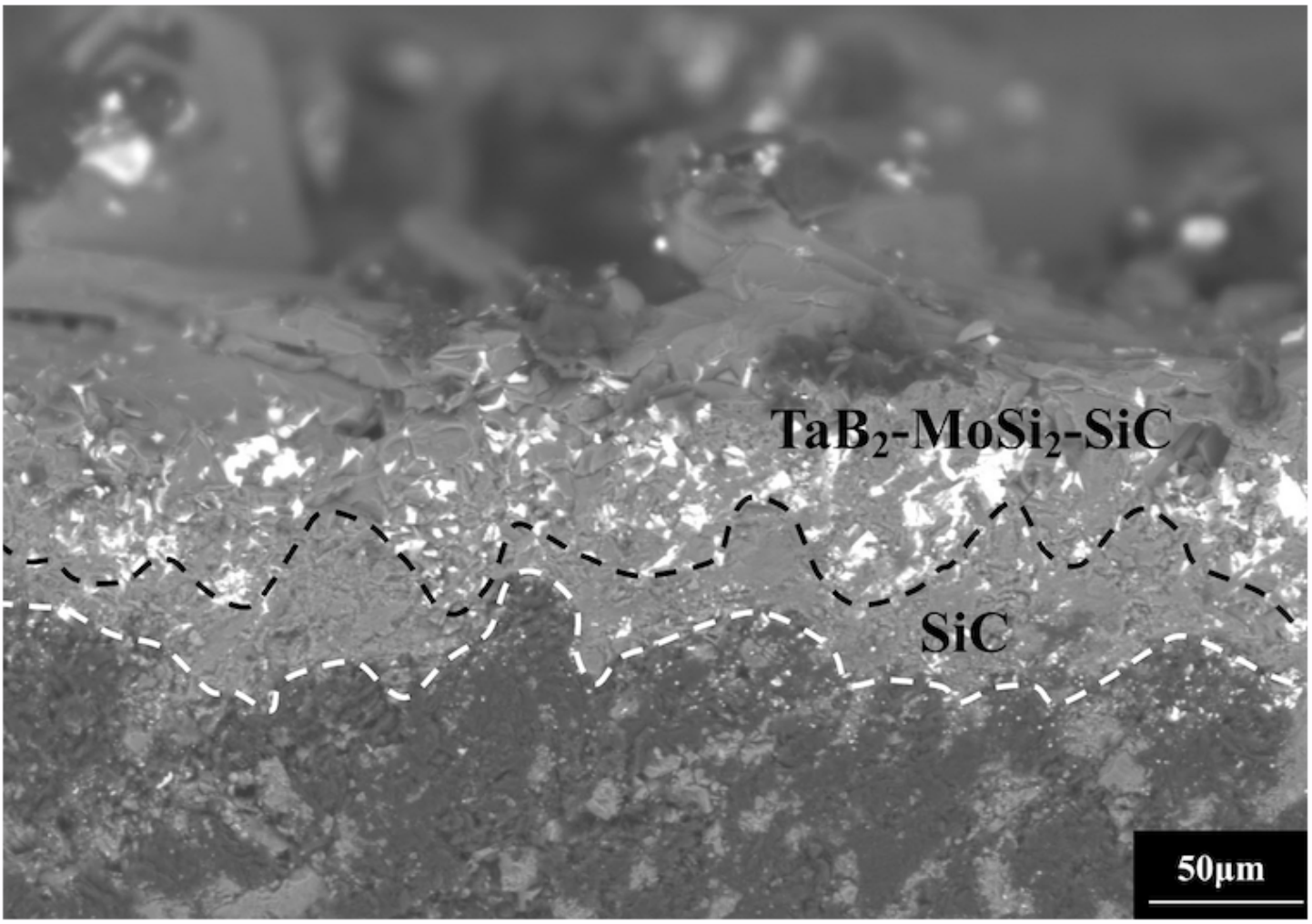

Figure 4

Cross-section morphology of the fabricated TaB2-MoSi2-SiC coating.

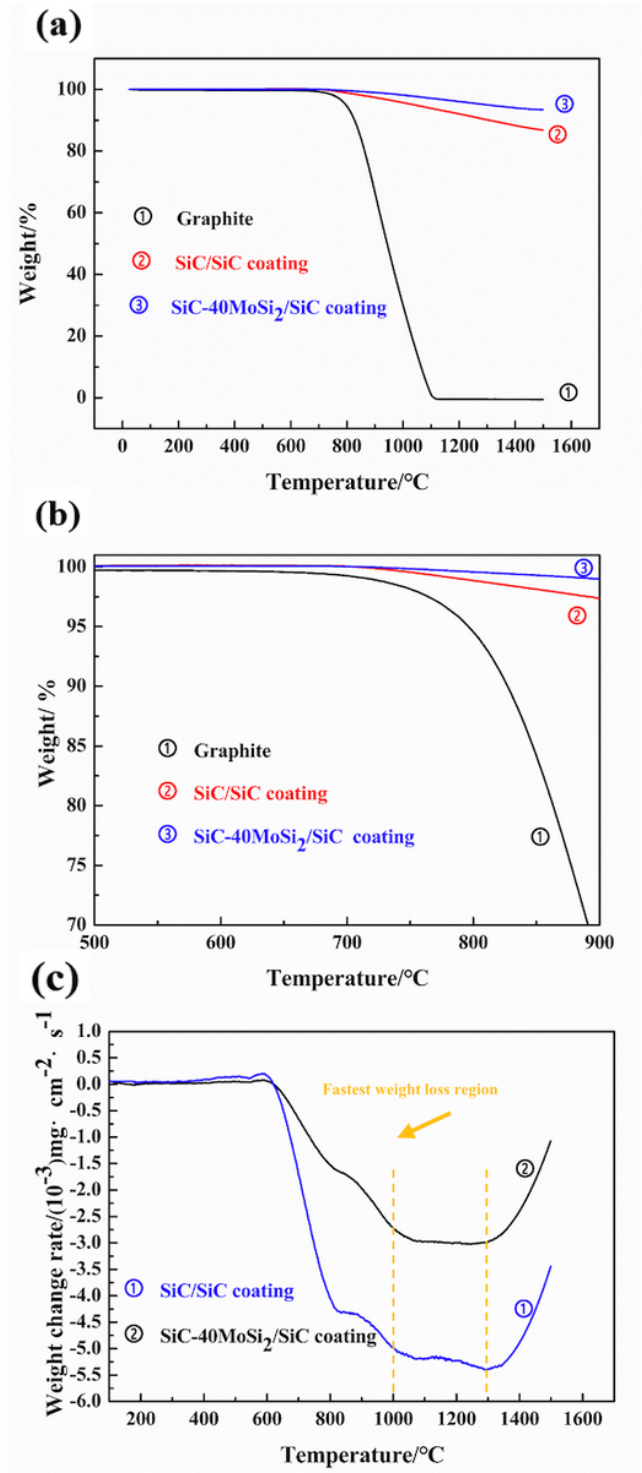

Figure 5

(a) TGA curves of the samples from room temperature to 1500 °C; (b) TGA curves of the samples from 500 °C to 900 °C; (c) weight loss rate curves of the samples from room temperature to 1500 °C.

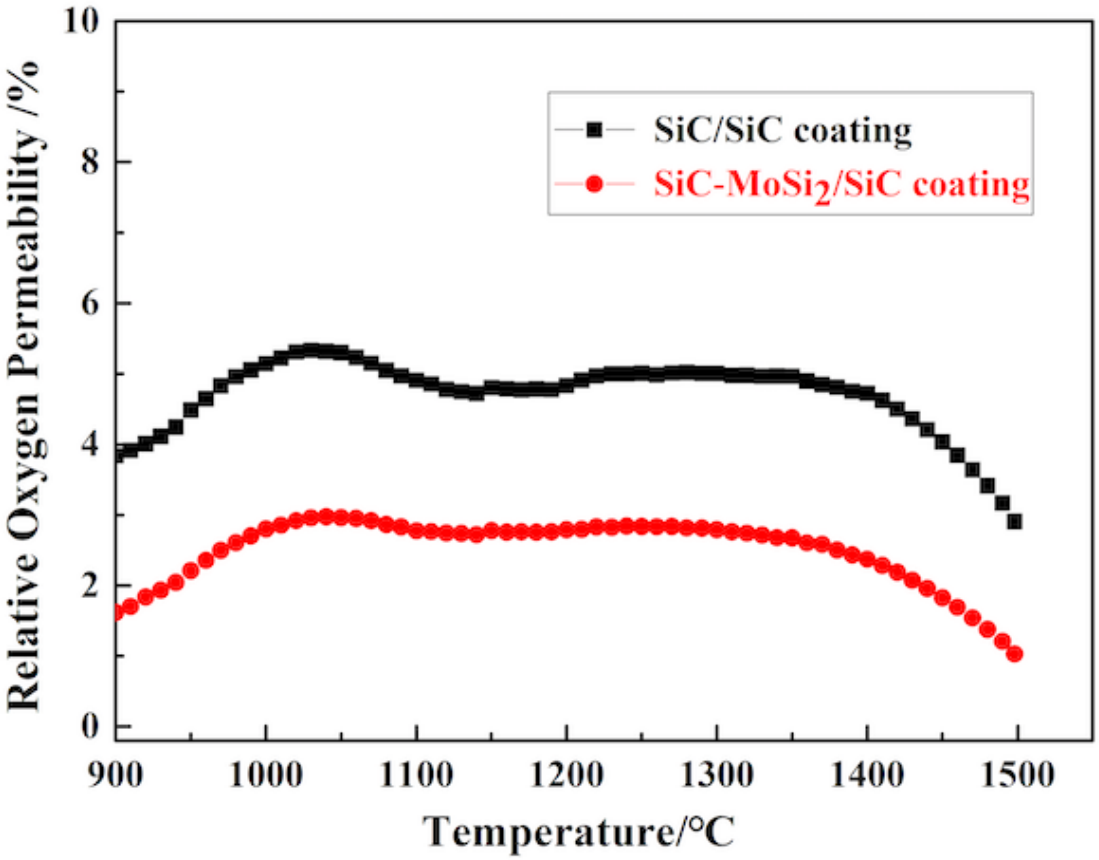

Figure 6

Relative oxygen permeability curves of the SiC/SiC coating and the MoSi2-SiC/SiC coating.

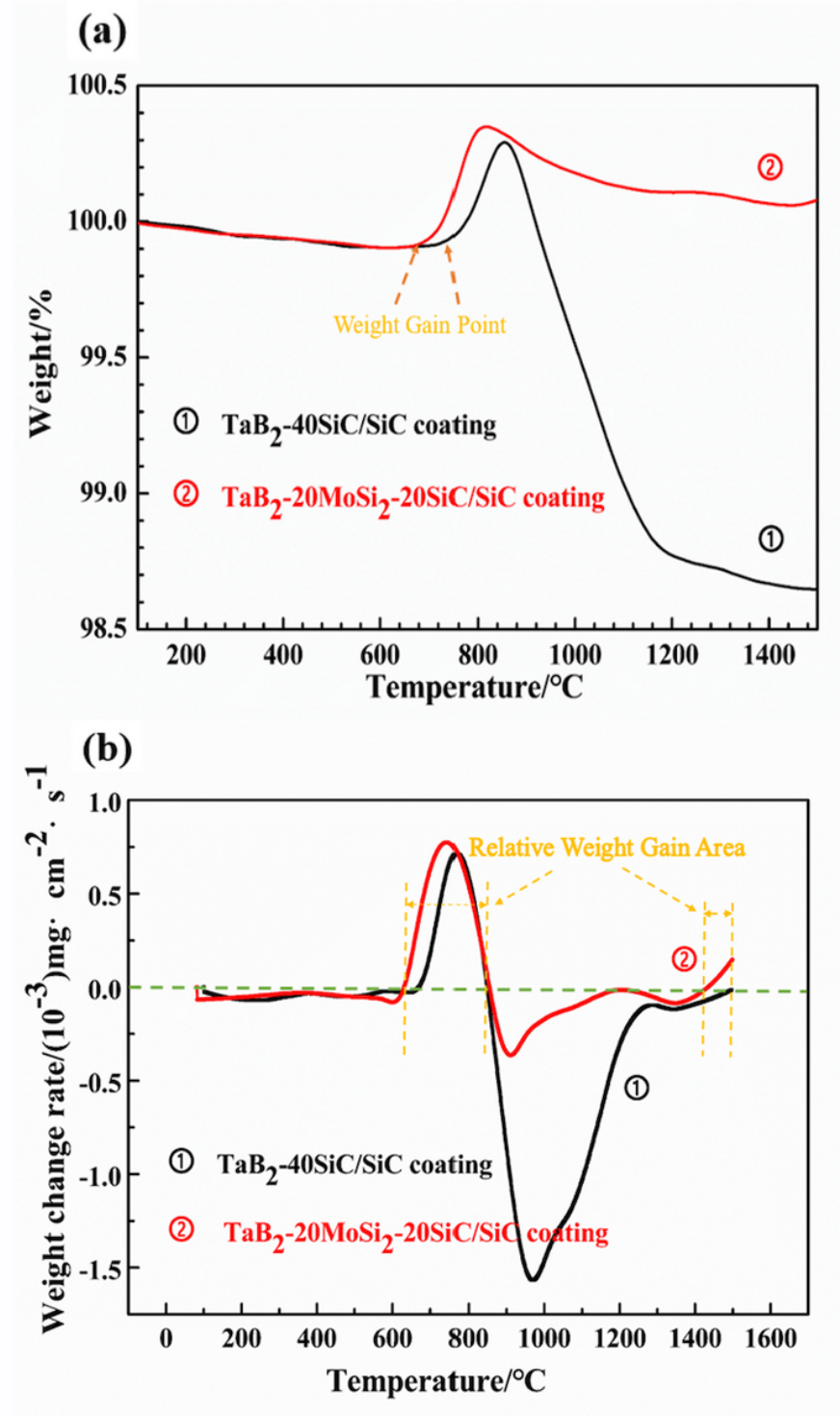

Figure 7

(a) TGA curves of the samples from room temperature to 1500 °C; (b) weight loss rate curves of the samples from 25 °C to 1500 °C.

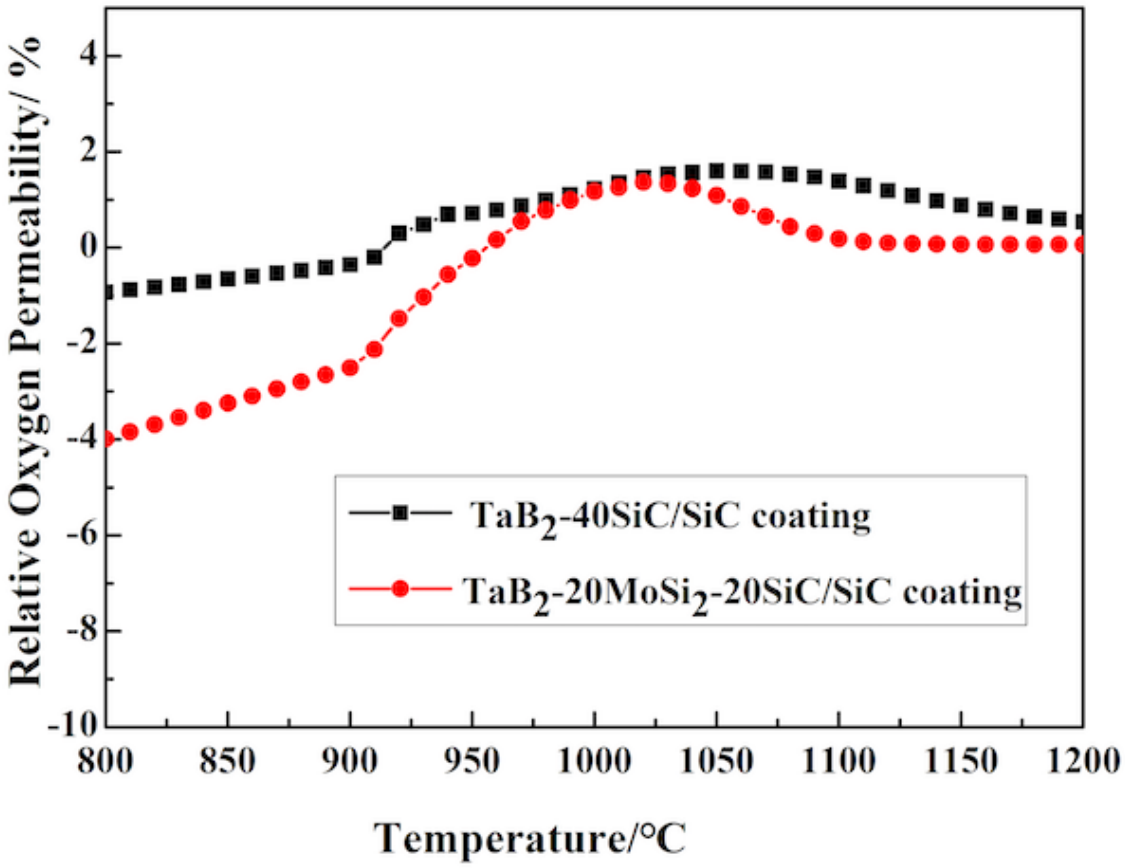

Figure 8

Relative oxygen permeability curves of the coatings from 800 °C to 1200 °C.

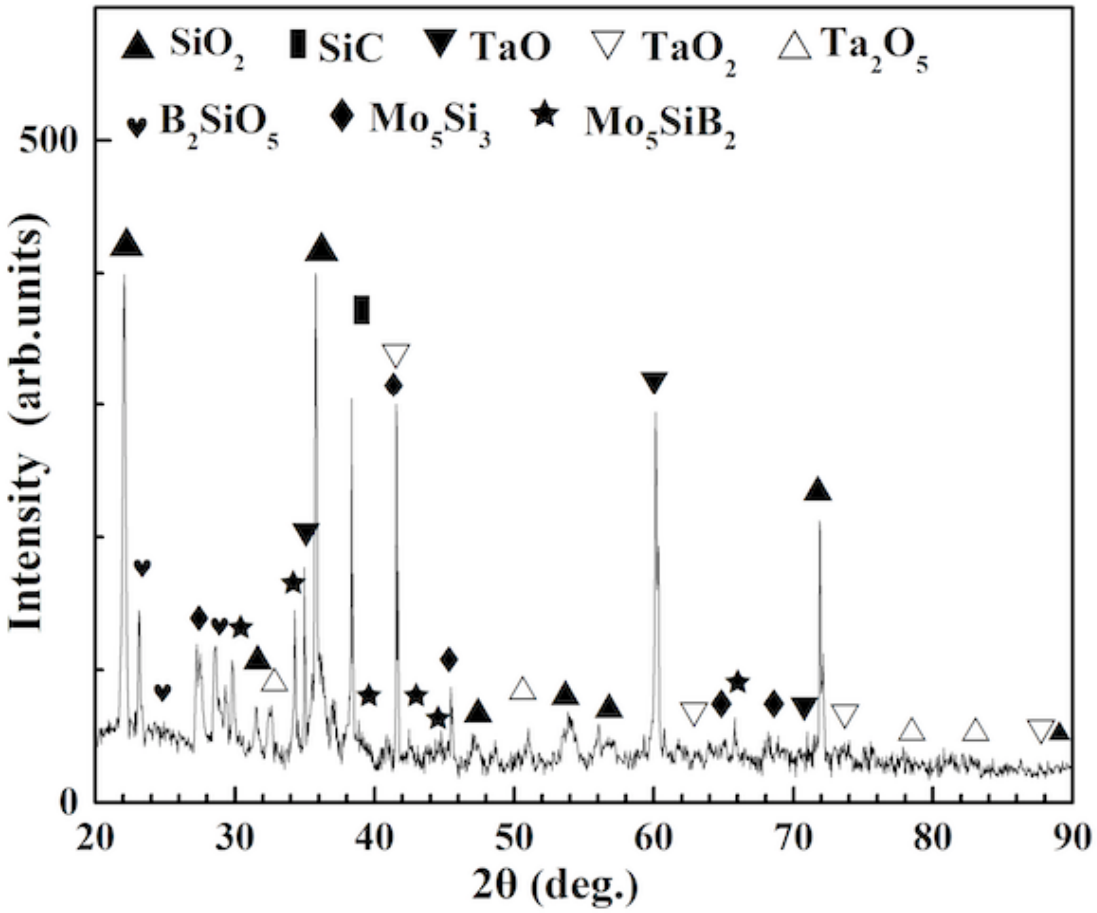

Figure 9

XRD pattern of the TaB2-MoSi2-SiC coating after oxidation.

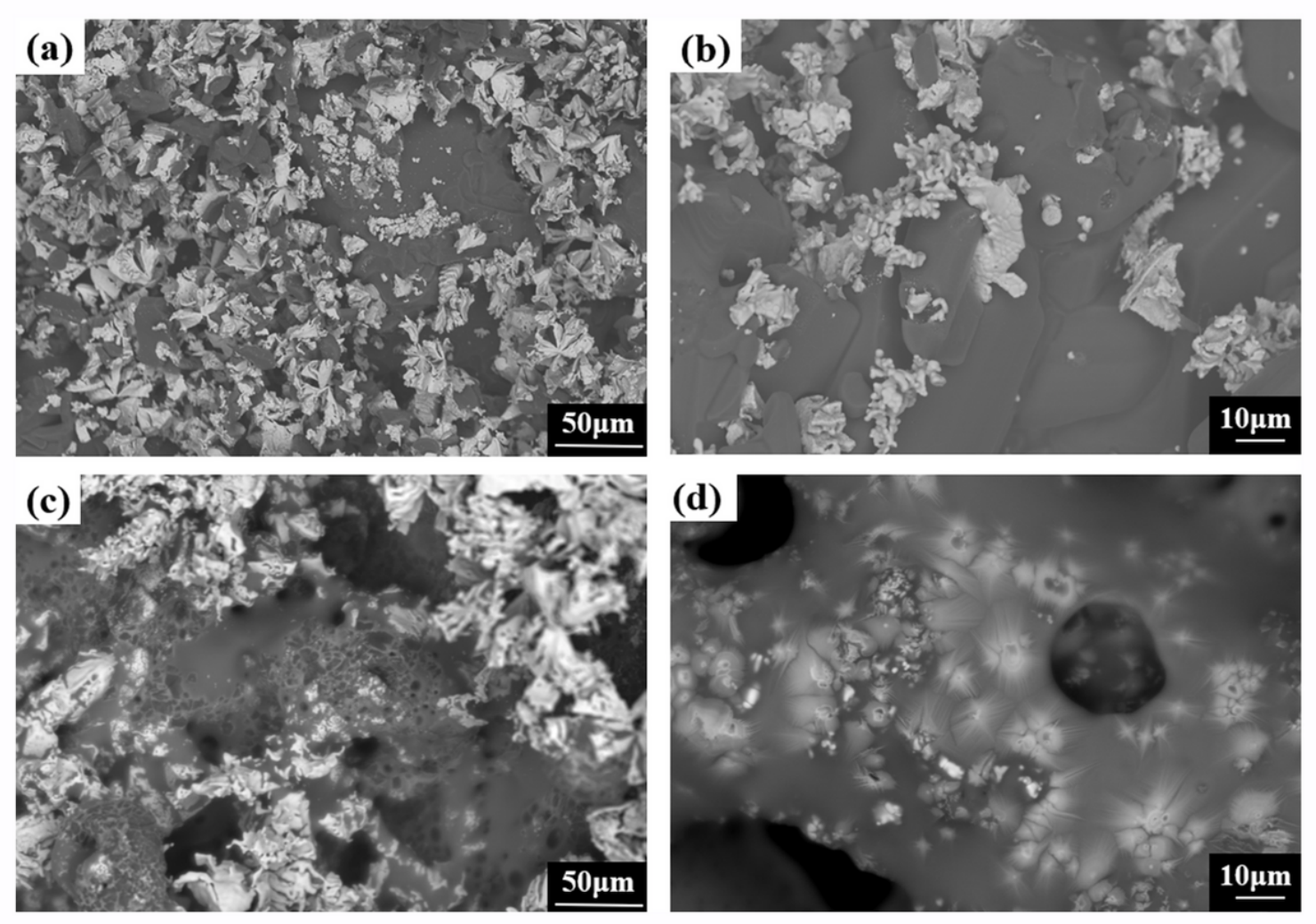

Figure 10

(a) the SEM micrographs of the TaB2-40wt.%SiC/SiC coating after TGA tests; (c) the SEM micrographs of the TaB2-20wt.%MoSi2-20wt.%SiC/SiC coating after TGA tests; (b), (d) the magnification of (a), (c).

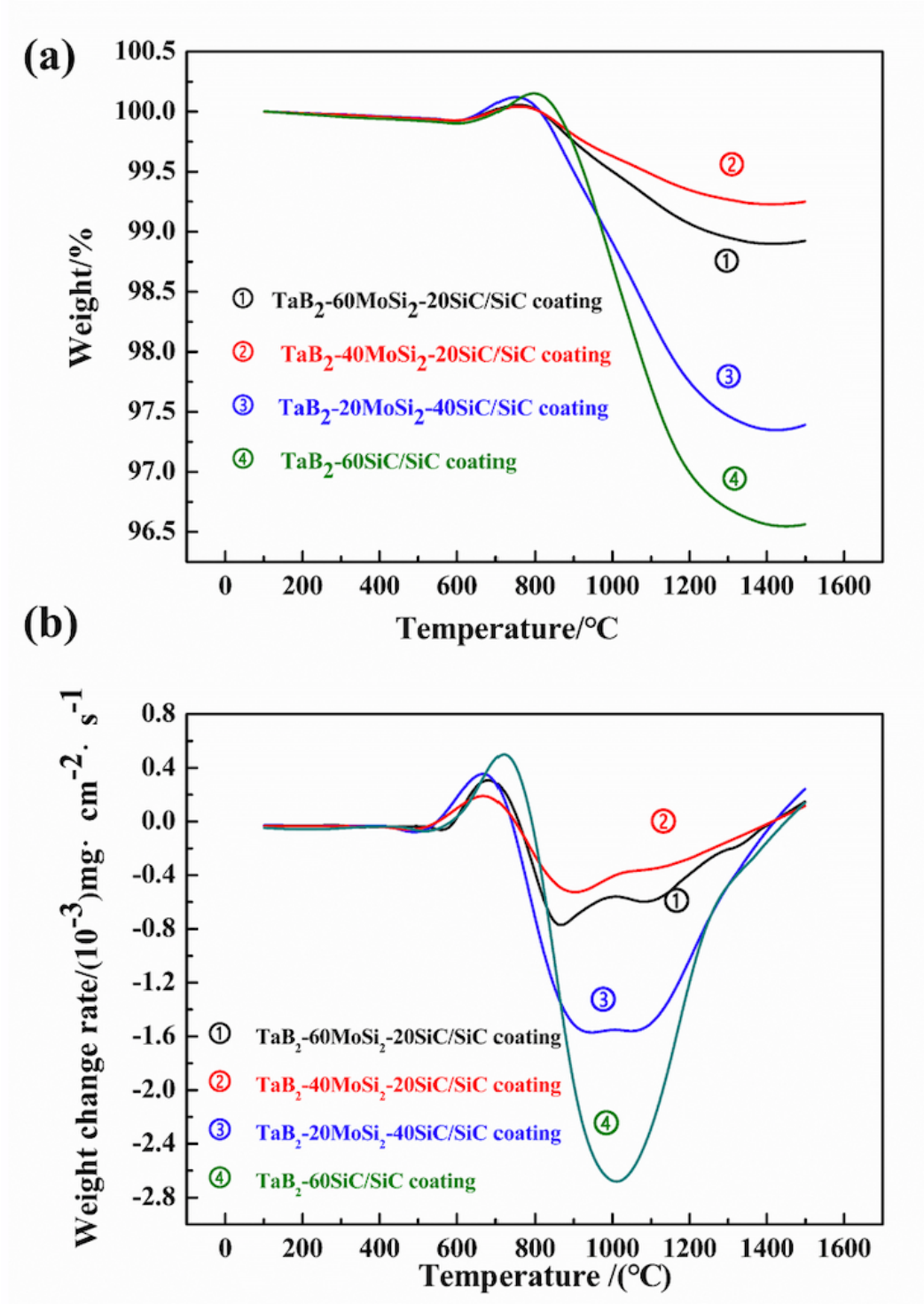

Figure 11

(a) TGA curves of the samples with different MoSi2 contents or TaB2 contents; (b) weight change rate curves of the samples with different MoSi2 contents or TaB2 contents.

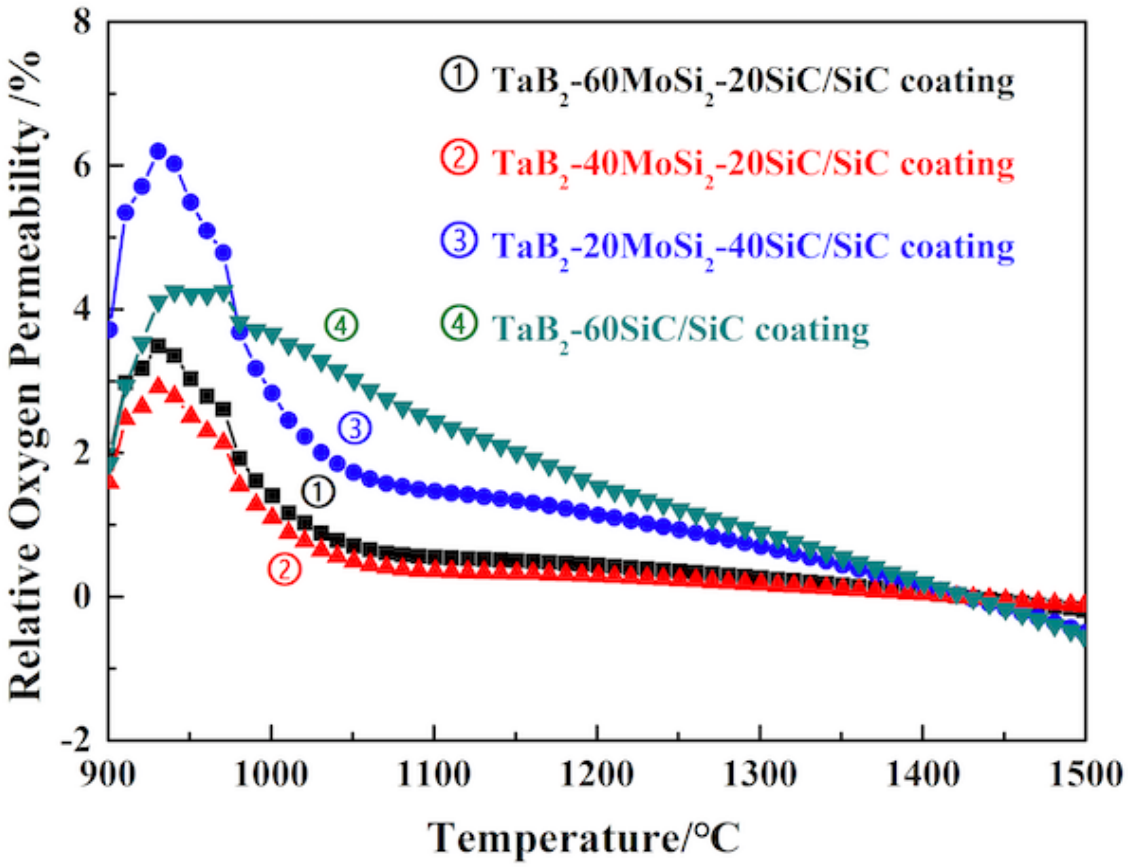

Figure 12

Relative oxygen permeability curves of the fabricated different coatings.

Figure 13

SEM micrographs of the 40wt.%TaB2-MoSi2-SiC/SiC coatings with different MoSi2 contents after oxidation at 1500 ℃ for 100 h, (a) 0 wt.%MoSi2, (b) 20 wt.%MoSi2, (c) 40 wt.%MoSi2; (d) SEM micrograph of the 20wt.%TaB2-60wt.%MoSi2-SiC/SiC coating after oxidation at 1500 ℃ for 100 h.

Figure 14

Surface EDS spectrum of the TaB2-MoSi2-SiC/SiC coating surface after isothermal oxidation test at 1500 ℃ for 100 h.